

## ARTICLE



# Transcriptome and unique cytokine microenvironment of Castleman disease

Anna Wing<sup>1,6</sup>, Jason Xu<sup>1,6</sup>, Wenzhao Meng<sup>2</sup>, Aaron M. Rosenfeld<sup>1,2</sup>, Elizabeth Y. Li<sup>1</sup>, Gerald Wertheim<sup>2,3</sup>, Michele Paessler<sup>2,3</sup>, Adam Bagg<sup>2</sup>, Dale Frank<sup>1,2</sup>, Kai Tan<sup>4</sup>, David T. Teachey<sup>4</sup>, Megan S. Lim<sup>2</sup>, Eline Luning Prak<sup>1,2</sup>, David C. Fajgenbaum<sup>5</sup> and Vinodh Pillai<sup>1,2,3</sup>✉

© The Author(s), under exclusive licence to United States & Canadian Academy of Pathology 2021

Castleman disease (CD) represents a group of rare, heterogeneous and poorly understood disorders that share characteristic histopathological features. Unicentric CD (UCD) typically involves a single enlarged lymph node whereas multicentric CD (MCD) involves multiple lymph node stations. To understand the cellular basis of CD, we undertook a multi-platform analysis using targeted RNA sequencing, RNA in-situ hybridization (ISH), and adaptive immune receptor rearrangements (AIRR) profiling of archived tissue from 26 UCD, 14 MCD, and 31 non-CD reactive controls. UCD showed differential expression and upregulation of follicular dendritic cell markers (CXCL13, clusterin), angiogenesis factors (LPL, DLL4), extracellular matrix remodeling factors (TGFB, SKIL, LOXL1, IL-1 $\beta$ , ADAM33, CLEC4A), complement components (C3, CR2) and germinal center activation markers (ZDHC2 and BLK) compared to controls. MCD showed upregulation of IL-6 (IL-6ST, OSMR and LIFR), IL-2, plasma cell differentiation (XBP1), FDC marker (CXCL13, clusterin), fibroblastic reticular cell cytokine (CCL21), angiogenesis factor (VEGF), and mTORC1 pathway genes compared to UCD and controls. ISH studies demonstrated that VEGF was increased in the follicular dendritic cell-predominant atretic follicles and the interfollicular macrophages of MCD compared to UCD and controls. IL-6 expression was higher along interfollicular vasculature-associated cells of MCD. Immune repertoire analysis revealed oligoclonal expansions of T-cell populations in MCD cases (2/6) and UCD cases (1/9) that are consistent with antigen-driven T cell activation. The findings highlight the unique genes, pathways and cell types involved in UCD and MCD. We identify potential novel targets in CD that may be harnessed for therapeutics.

*Modern Pathology* (2022) 35:451–461; <https://doi.org/10.1038/s41379-021-00950-3>

## INTRODUCTION

Castleman disease (CD) is broadly categorized into unicentric and multicentric disease.<sup>1</sup> Unicentric CD (UCD) has minimal systemic symptoms, is restricted to a single lymph node station, and is generally cured by excisional surgery.<sup>2–4</sup> Multicentric CD (MCD) is characterized by widespread lymphadenopathy, systemic inflammation, and multi-system organ dysfunction and is treated by immunotherapy and chemotherapy.<sup>5</sup> MCD is further subclassified based on etiologies and treatment approaches: human herpesvirus-8 (HHV-8)-associated, Polyneuropathy, Organomegaly, Endocrinopathy, Monoclonal protein and Skin changes (POEMS)-associated MCD and HHV-8 negative idiopathic MCD (iMCD). iMCD includes newly described variants such as Thrombocytopenia, Anemia, Fever, Reticulin fibrosis and Organomegaly (iMCD-TAFRO).<sup>6</sup> The distinction between the various entities is difficult on morphologic criteria alone and requires integration of clinical, radiologic and pathologic findings.<sup>7</sup>

Characteristic histopathological features of CD range from a hyaline vascular pattern to a plasmacytic pattern. UCD lymph nodes often have FDC-enriched atretic follicles with shared mantle

zones, and prominent interfollicular vascularity with hyalinization (hyaline vascular pattern). In contrast, MCD contain atretic or hyperplastic follicles and increased interfollicular vascularity and/or plasmacytosis that can be described as hyaline-vascular/hypervascular, plasmacytic or mixed.<sup>8</sup> The atretic follicles are enriched in follicular dendritic cells while the mantle zones are enriched in B cells. The interfollicular zones are variably enriched in activated endothelial cells, plasma cells, fibroblasts, macrophages and lymphocytes. Though the morphological characteristics of CD are well described, the key cellular and molecular pathways underlying the pathogenesis of these features have not been elucidated.

MCD is characterized by a systemic hypercytokinemia that includes IL-6, VEGF, IL-2, TNF $\alpha$ , IL-10, and CXCL13.<sup>9,10</sup> The source of hypercytokinemia depends on type of MCD. In HHV-8-associated MCD, hypercytokinemia is driven by the virus<sup>11,12</sup> while in POEMS-associated MCD, it is produced by monoclonal plasma cells. IL-6 is critical to the pathogenesis of the iMCD. Targeting IL-6 with monoclonal antibodies tocilizumab or siltuximab ameliorates iMCD symptoms in one-third to one-half of patients.<sup>13,14</sup> VEGF is

<sup>1</sup>Perelman School of Medicine, University of Pennsylvania, Philadelphia, PA, USA. <sup>2</sup>Department of Pathology and Laboratory Medicine, University of Pennsylvania, Philadelphia, USA. <sup>3</sup>Division of Hematopathology, The Children's Hospital of Philadelphia, Philadelphia, PA, USA. <sup>4</sup>Department of Pediatrics, The Children's Hospital of Philadelphia, Philadelphia, PA, USA. <sup>5</sup>Center for Cytokine Storm Treatment and Laboratory, Department of Medicine, University of Pennsylvania, Philadelphia, USA. <sup>6</sup>These authors contributed equally: Anna Wing, Jason Xu. ✉email: pillai1@chop.edu

Received: 31 July 2021 Revised: 5 October 2021 Accepted: 5 October 2021  
Published online: 22 October 2021

another important cytokine that is markedly increased in serum of iMCD and POEMS.<sup>8,15</sup> Though the central role of hypercytokinemia in mediating the symptoms of iMCD is known, the etiology is unclear. IL-6 is primarily produced by T cells, macrophages and VEGF is produced by macrophages, platelets, and granulocytes, but both cytokines can be produced by a variety of other immune and stromal cells. Clonal populations of stromal cells or plasma cells are reported by some studies,<sup>16,17</sup> but not others.<sup>9,18</sup> Cytogenetic abnormalities and monoclonality (by human androgen receptor methylation assay) are noted occasionally in UCD.<sup>19</sup> Targeted DNA sequencing studies show mutations of *FAS*,<sup>20</sup> *ETS1*, *PTPN6*, *TGFB2*,<sup>21</sup> *MEFV*,<sup>22</sup> *NCOA4*,<sup>23</sup> and *PDGFRB*<sup>24</sup> mutations in UCD and MCD. A transcriptome analysis of CD cases has not been reported.

To better define the cells and molecules that contribute to disease pathogenesis in CD, we utilized RNA in-situ hybridization, RNA sequencing and immune repertoire profiling of archived frozen and formalin fixed paraffin embedded (FFPE) tissue. We analyzed these data to systematically compare the lymph node of UCD and MCD. We reasoned this comparison of UCD, MCD and reactive lymph nodes would provide novel and important findings given the characteristic histomorphological changes in lymph nodes that are essential for diagnosing CD. We identified several differentially expressed genes and pathways in UCD and MCD that could be harnessed for therapeutic purposes.

## METHODS

### Cases and controls

Cases of CD and non-CD lymph node controls were identified from the pathology archives at the Children's Hospital of Philadelphia and the Hospital of the University of Pennsylvania. The study was approved by the Institutional review boards and performed in accordance with the Declaration of Helsinki. Unicentricity, lack of systemic symptoms and histological features of attenuated follicles with shared concentric mantle zones penetrated by hyalinized vessels were considered as diagnostic features of UCD. Multicentricity, systemic symptoms, cytopenias, hypergammaglobulinemia, serous effusions, atretic or hyperplastic follicles, and interfollicular plasmacytosis or hypervascularity were considered as diagnostic features of MCD. Subtypes of MCD were determined from clinicopathologic data. Lymph nodes with reactive follicular hyperplasia, Castlemann-like changes, sinus histiocytosis and acute/chronic inflammation were identified as non-CD controls. Lymph nodes with castlemann-like changes such as attenuated germinal centers with expanded mantle zones (without hyalinization or shared mantle zones) were appropriate controls for morphological features of UCD. Reactive follicular hyperplasia, sinus histiocytosis and plasmacytosis were controls for morphological features of MCD. Clinical immunophenotypic analyses for neoplastic B cell or T cell populations were negative in all the cases. Cases were reviewed and assessed utilizing clinicopathologic criteria for MCD<sup>8</sup> by hematopathologists. Information from pathology reports, histological review, radiological studies, laboratory results and clinical course were integrated to determine the final clinicopathologic diagnosis. RNAseq, RNAISH, AIRRseq were performed based on tissue available in each case.

### RNA sequencing

Targeted RNAseq analysis was successfully performed on limited and archived FFPE tissues using the HTG EdgeSeq platform (HTG Molecular Diagnostics, Arizona).<sup>25</sup> This platform shows high correlation with other RNAseq platforms and a low failure rate with FFPE.<sup>26,27</sup> The Immune Response Panel was used for the gene expression analysis of 2003 autoimmunity-related gene (Complete gene list in supplemental file 1) The HTG EdgeSeq technology is based on the nuclease exclusion assay where an excess of nuclease protection probes (NPP) complementary to each mRNA hybridize to their targets. S1 nuclease removes unhybridized probes and RNA, leaving only NPPs hybridized to their targets at a 1:1 ratio. FFPE lymph node tissue from CD cases and controls were used to make 5 µm thin sections. Tissue fragments were separated from the slides and dissolved in lysis buffer by addition of proteinase K at 50 °C with shaking for 3 h. 35 µl of processed tissue samples were transferred onto the HTG EdgeSeq instrument for hybridization and S1 nuclease reaction. Molecular

bar codes and adapters were added, and the material was amplified using a thermocycler. Libraries were purified with AMPure XP magnetic beads (Beckman Coulter, USA) and quantified using KAPA BioSystems qPCR kit (Roche, USA). Samples were sequenced using high output Next-Seq 500/550 (single end, 75 bp, read length) (Illumina USA) according to the manufacturers protocol. FASTQ files were parsed on HTG EdgeSeq parser constructing a gene expression count matrix for each gene and each sample. They were merged to form a single output file containing all genes and all counts. Downstream analysis of RNA data was performed using HTG Edgeseq Reveal, a web-based data analysis software. Gene counts were normalized using quantile normalization (QN) based on best practice guidelines previously applied with the HTG EdgeSeq targeted immunology panel.<sup>28</sup> Quality control of RNA sequencing data was performed in line with recommendations from HTG, to satisfy cut-offs for sample quality, sufficient read depth and minimal expression variability across probes. Differential expression was assessed using DESeq2 package (Python, within Reveal software, 2020 version). Additional data analysis was performed in R.

### Identification of differentially expressed genes in R

Read counts were filtered to include only genes with a read count of at least 5 in greater than 10% of the samples. Patients were grouped by UCD, MCD, and control categories. Differential expression analysis was performed using Limma-Voom.<sup>29</sup> Log fold change 0.5 and false discovery rate of 20% were used. Formally, the contrast matrix included the following comparisons: UCD–MCD, UCD–Controls, MCD–Controls and the design matrix specified the following model for expected log-counts per million ( $y_{gi}$ ) for gene G and RNA-seq sample i:  $E(y_{gi}) = \mu_{gi} = \sim 0 + \text{disease}$

### Pathway enrichment analysis

Pathway enrichment analysis for differentially expressed (DE) genes was performed using Metascape, a web-based tool that combines functional enrichment, interactome analysis, gene annotation, and membership search of 40 independent knowledge databases.<sup>30</sup> It uses the hypergeometric test with Benjamini-Hochberg p-value correction and clustering of similar enriched terms in core gene sets: pathway (Reactome Gene Sets, Canonical Pathways, BioCarta Gene Sets, GO Biological Processes, Hallmark Gene Sets, and KEGG Pathway), functional set (GO Molecular Functions), structural complex (GO Cellular Components, KEGG Structural Complex, and CORUM Protein Complex), and signature module (immunologic signatures, oncogenic signatures, and chemical and genetic perturbations). Terms with a P-value of < 0.01, a minimum count of 3 and an enrichment factor of >1.5 (the enrichment factor is the ratio of the observed count to the count expected by chance) were collected and grouped into clusters based on their membership similarities. Kappa scores were used as the similarity metric when performing hierarchical clustering of the enriched terms; sub-trees with a similarity of >0.3 were considered a cluster. Representative terms within a cluster was selected as the ones representing the cluster. Gene Set Enrichment Analysis was also performed<sup>31</sup> and showed similar results as Metascape.

### Protein–protein interaction (PPI) network

PPI networks of intersection DEGs were analyzed with the threshold (combined\_score > 0.4) using the STRING tool, which can provide interactions across matched proteins.<sup>32</sup> Subsequently, molecular complex detection (MCODE) was applied to extract sub-networks in PPI networks with default algorithms (degree cut-off of 2, node score cut-off of 0.2, K-Core of 2, and max. depth of 100).<sup>33</sup>

### Immunohistochemistry and RNA in situ hybridization

FFPE tissue were utilized for immunohistochemistry (IHC) and RNAscope analysis. IHC for CD138 (Dako MI15 clone, 1:200 dilution), CD163 (Leica 106D, 1:800), CD123 (BD Pharmingen 9F5, 1:110), CD20 (Dako LS26, 1:1000), CD31 (Dako JC70A, 1:200), and vimentin (Dako V9, 1:50) were performed. Staining was performed on a Bond Max automated staining system (Leica Biosystems, Germany) using the Bond Refine polymer staining kit (Leica Biosystems, Germany) according to manufacturer protocol. RNA in situ hybridization (ISH) was performed using RNAscope<sup>®</sup> 2.5 HD Duplex Assay (ACDBio) according to the manufacturer's instructions with probes for VEGF, IL-6, IL-6R, IL-1β, IL-2, IL-8, IL-10, and TNFα obtained from ACDBio. A dual ISH-IHC protocol was validated to simultaneously stain selected FFPE tissue slides with immunohistochemistry antibodies and RNAscope<sup>®</sup> probes. Stained slides were digitally scanned at 20×

**Table 1.** Characteristics of cases and controls. Age, sex, site of involvement, histological subtype and assessments performed in various groups.

Diagnosis	Age range in years (median)	M:F	Involvement	Subtype (n)	RNAseq:RNAISH:immunoseq assessment (n)
UCD	4–54(16.6)	14:12	Cervical-15 Mediastinal-5 Inguinal-2 Mesenteric-2 Axillary- 1 Soft tissue-1	Hyaline vascular- 23 Mixed/Plasma cell -3	21:17:6
MCD	12–71 (15)	8:6	Multiple sites	Plasma cell-8 TAFRO- 3 HIV-1 POEMS-2	12:8:8
Reactive	2–48 (11)	23:8	Cervical-15 Mesenteric-4 Mediastinal-3 Axillary-5 Inguinal-2 Retroperitoneal-1	Castleman like- 12 Follicular hyperplasia- 5 Infectious- 11 Dermatopathic-1 Sinus histiocytosis-2	35:11:5

magnification on an Aperio CS-O slide scanner (Leica Biosystems, Germany). Appropriate positive and negative controls were utilized per the manufacturer's recommendation to ensure RNA integrity and exclude background signal. RNAscope ISH was manually scored using a semi quantitative scale from 0 to 4 following the manufacturer's guidelines (ACDBio). A score of zero is no staining or < 1 dot signal/10 cells. 1+ signal is 1–3 dots/cell. 2+ signal is 4–9 dots/cell with no or very few dot clusters. 3+ signal is 10–15 dots/cell and with < 10% of dots in clusters. 4+ signal is >15 dots/cell and >10% dots are in clusters. Lymph node regions such as the germinal center, mantle zone, and interfollicular areas were scored separately to analyze site-specific differences in cytokine expression.

#### Human TRBV and IGHV gene rearrangement sequencing

Adaptive immune receptor rearrangements (AIRR-seq) were sequenced from bulk genomic(g)DNA. Genomic DNA was extracted from OCT embedded frozen samples using the Qiagen Genra DNA purification kit (Qiagen, Germantown, MD, Cat. No.158689). Sequences were generated from gDNA using primers that were situated near FR2 and J $\beta$  (BIOMED2) for TRBV sequencing<sup>34</sup> and, FR1 and JH (BIOMED2) for IGH rearrangement sequencing. Samples were amplified in duplicate (2 biological replicates per sample) and the input DNA was 400 ng per replicate. TCRBV and IGH rearrangements<sup>35</sup> generated from these PCRs were subjected to second-round amplification to generate sequencing libraries using the Illumina Nextera XT (2  $\times$ 300 bp) paired end kit, sequenced and quality filtered as described previously.<sup>35,36</sup> 2  $\times$ 300 bp paired end sequencing was performed on an Illumina MiSeq instrument. ImmuneDB<sup>37</sup> was used to group related sequences into clonotypes and visualize immune repertoire features, generate spectratype, somatic hypermutation and clone rank plots, described previously.<sup>35,38</sup>

#### Processing and analysis of AIRR-seq data

Raw data from the MiSeq were quality controlled with PRESTO as described previously<sup>35</sup> and gene assignment and alignment were performed with IgBLAST.<sup>39</sup> ImmuneDB<sup>37</sup> was used to group related sequences into clonotypes as described in TCR<sup>38</sup> and BCR.<sup>40</sup> Further visualization immune repertoire features including ranking of the top 20 copy clones and somatic hypermutation analysis, described previously.<sup>35,38</sup> Raw TRB and IGH gene rearrangement data are available on SRA under project number PRJNA750097.

## RESULTS

### Clinicopathologic characteristics of study cohort

Twenty six UCD, fourteen MCD, and thirty one non-CD reactive lymph nodes were identified from archives of the Children's Hospital of Philadelphia and the Hospital of University of Pennsylvania (Table 1). CD patients ranged from 2 to 71 years in the age but the median age was 15 due to predominance of adolescent and young adult cases in our cohort. There were no differences in histologic features between adolescent and adult cases. The male to female ratio of approximately 1:1 is consistent

with prior reports.<sup>41,42</sup> Males were overrepresented among control reactive nodes. UCD involved a single node or multiple nodes within the same lymph node station and presented mostly with local compression symptoms and no systemic symptoms. The cervical region were the most common site of involvement in UCD (58%) and reactive (48%) categories. Most UCD patients responded to single surgical resection while two patients needed a second resection for recurrent disease. HHV-8 testing (serology and/or immunohistochemistry) was negative in all cases. One reactive node and one MCD were known to be HIV-positive before biopsy. MCD patients frequently needed systemic therapy with steroids, immunotherapy and chemotherapy. Lymph nodes involved by UCD showed predominantly hyaline vascular pattern (88%). Mixed or plasma cell pattern were noted in a minority (12%). MCD lymph nodes showed predominantly plasma cell pattern (57%). MCD subtypes included three TAFRO, two POEMS and one HIV-associated (Table 1 and Supplementary Table 1). Non-CD reactive lymph nodes included those with non-specific Castleman-like features (39%), and acute/chronic inflammation (35%).

### Transcriptome analysis of UCD and MCD reveals upregulation of unique genes and pathways

Targeted RNA sequencing of 2003 immune-response and autoimmunity-associated genes were performed using FFPE tissue sections. All CD cases passed minimal quality control requirements for RNA degradation, read depth and expression variability. RNAseq assesses both the cellular and stromal microenvironment of lymph nodes in CD. DE gene analysis of UCD compared to reactive controls revealed 71 candidates (Fig. 1A and supplementary file 2). The top twenty most upregulated and DE genes in UCD included follicular dendritic cell markers CXCL13, clusterin and cytokines CXCR4 and IL-1 $\beta$  (Fig. 1B). Many genes involved in extracellular matrix modification pathways were noted: TGF $\beta$ 3, SKIL, LOX11, IL-1 $\beta$ , ADAM33, CLEC4A and SERPIN1. Angiogenesis factors LPL, DLL4, complement pathway components C3, CR2 and germinal center B cell activation molecules B cell tyrosine kinase BLK and ZDHHC2 also were among the top twenty DE genes. Metascape gene enrichment analysis of all DE genes in UCD (vs reactive control) identified enrichment of core gene sets of inflammatory response, cytokine signaling, complement cascade, angiogenesis, extracellular matrix remodeling, lymphocyte proliferation, and cell cycle (Fig. 1C). Protein–protein interaction enrichment analysis identified a C3–CXCL4–CXCL13–CXCL9–CXCL10 axis that was differentially expressed. Genes downregulated in UCD included proteasome components USP18, immune suppressive molecules LAG3 and PD1-L1, CEBPA, cytokines CXCL9, CXCL10, apoptosis inducer FAS, and STAT1 (Supplementary

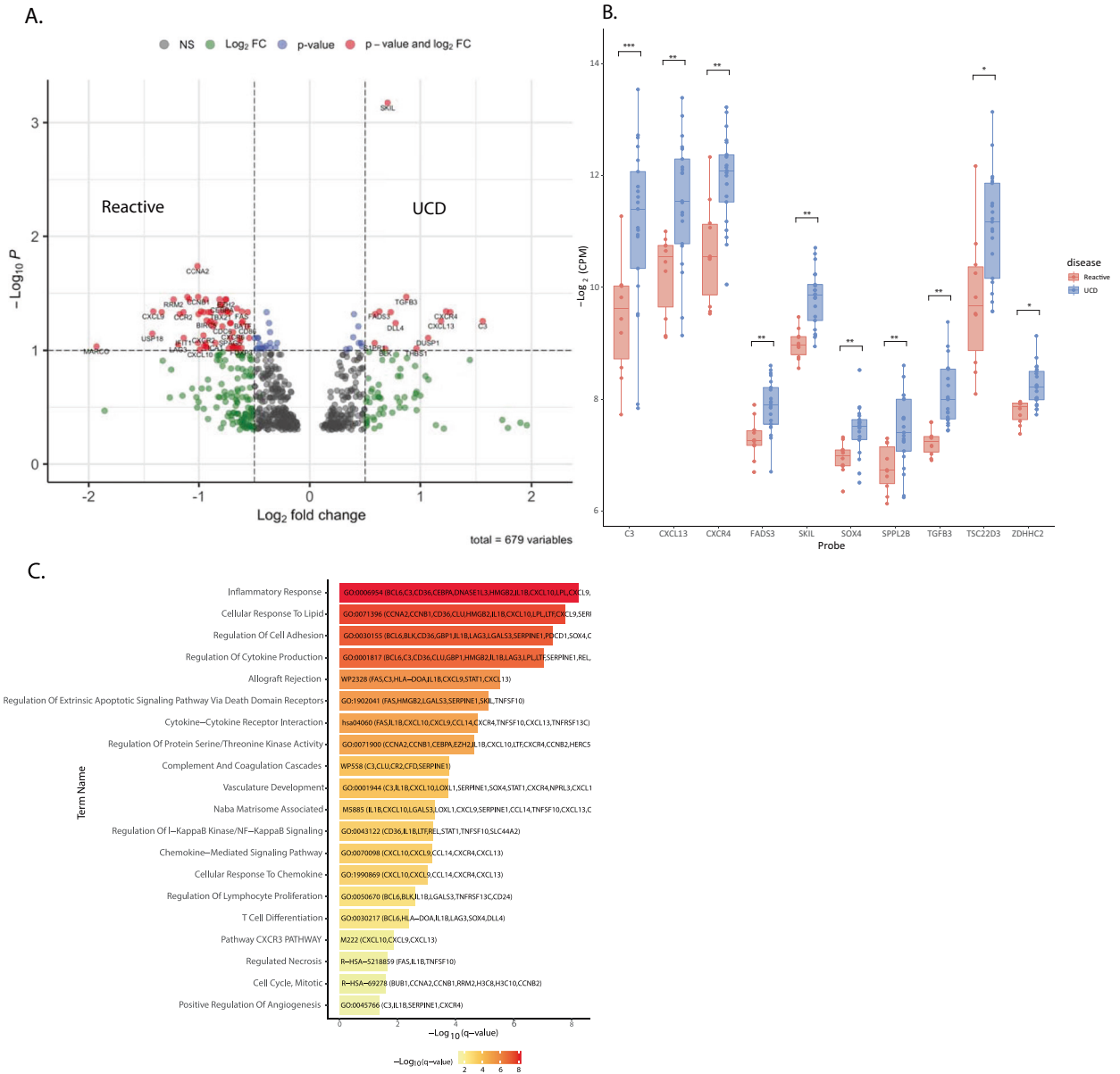


**Fig. 1 Unique genes and pathways of UCD compared to non-CD reactive control. A** Volcano plot of significantly DE and upregulated genes. Genes in red represent those that satisfied log fold change > 0.5, and false discovery rate of 20%. **B** Box plots of the top 10 DE genes. Y axis represents log<sub>2</sub> transformed transcripts per million. Boxes represent 25-75th percentile of expression and whiskers represent minimum and maximum data points. **C** Enriched pathways and DE genes in each pathway.

Fig. 1A). Many of the genes upregulated in reactive nodes were related to normal lymphoid or myeloid differentiation and function.

Gene expression analysis of MCD vs. reactive control lymph nodes revealed 37 DE genes (Fig. 2A and supplementary file 2). Similar to UCD, genes upregulated in MCD included FDC markers CXCL13 and CLU, complement pathway member CR2 and germinal center differentiation gene ZDHHC2. However, several other genes unique to MCD were identified. Fibroblastic reticular cell marker and cytokine CCL21, cell cycling gene CCND2, IL-6 pathway genes IL-6ST, OSMR and LIFR were among the top DE genes (Fig. 2B). Metascape analysis of DE genes in MCD (vs reactive control) showed enrichment of various core gene sets such as VEGF signaling, chemokine signaling, immune response, complement cascade, chemotaxis, IL-6 signaling pathway and T cell activation (Fig. 2C).

We then compared UCD and MCD with each other to determine uniquely expressed genes and pathways. 71 DE genes (Fig. 3A and supplementary file 2) were identified. Upregulated genes in MCD included T-cell activation marker IL-2RA, plasma cell differentiation transcription factor XBP1, cell cyclin genes CCNA1, CCNB2, RAP1A pathway while those upregulated in UCD included SKIL, BLK, RNASET1, MAPK3A1, TLR1, CLEC4A (Fig. 3B). Metascape analysis of DE genes revealed enrichment of core gene sets of lymphocyte and macrophage activation, inflammation, IL-6 pathway, angiogenesis, cytokine (IL-4, IL-13 and IL-1) signaling, and cell cycle (Fig. 3C).

**Increased IL-6 expression by endothelial cells in MCD**

Given the reported importance of IL-6, VEGF, IL-2 and other cytokines to MCD<sup>9</sup> and in our RNAseq data, we utilized RNA ISH to identify the lymph node structures and cells expressing these cytokines. RNA ISH is more sensitive and specific than IHC and

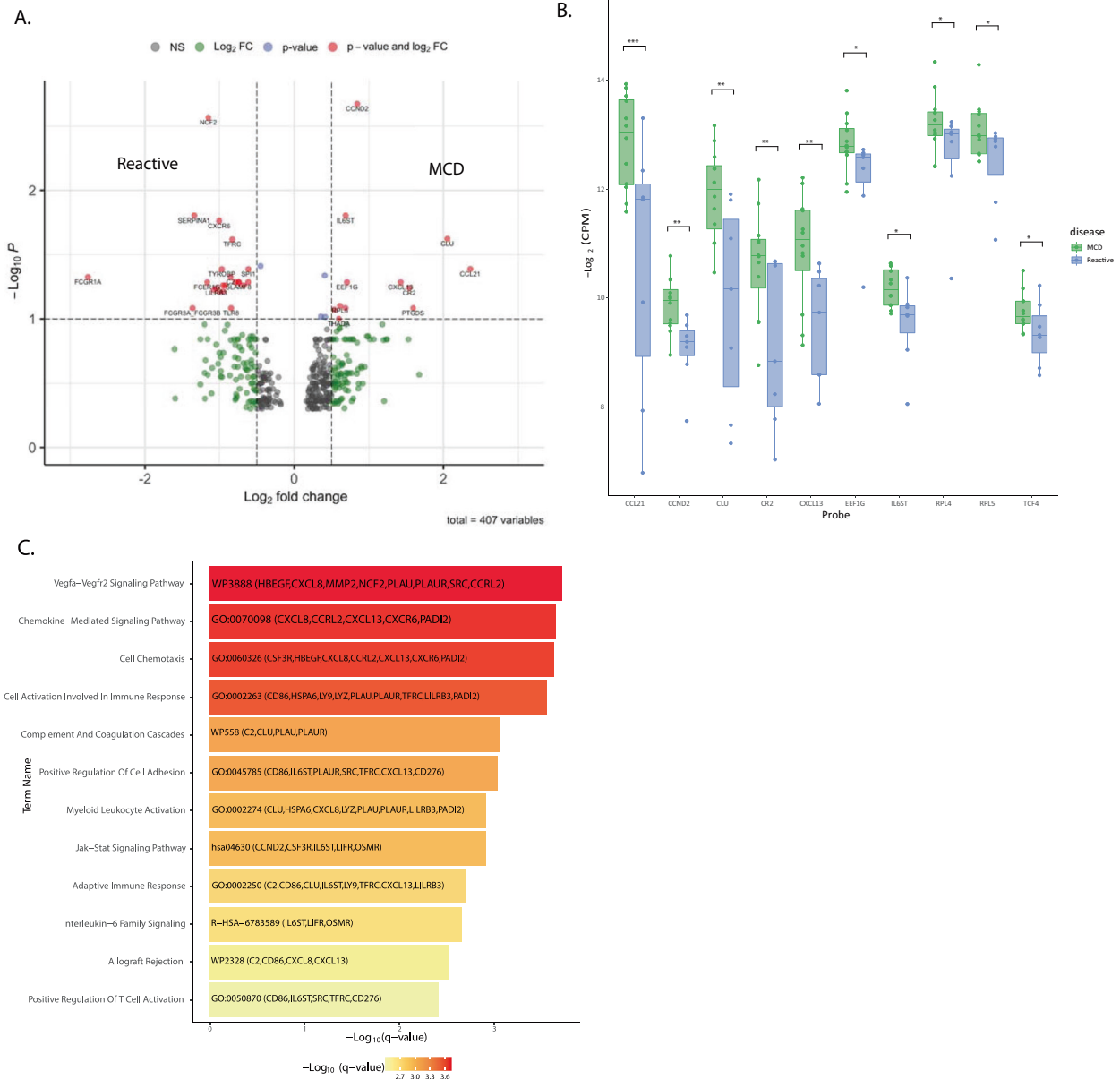


**Fig. 2 Unique genes and pathways of MCD compared to non-CD reactive control. A** Volcano plot of significantly DE and upregulated genes. Genes in red represent those that satisfied  $\text{log}$  fold change  $> 0.5$ , and false discovery rate of 20%. **B** Box plots of top 10 DE genes upregulated in MCD versus reactive. Y axis represents  $\text{log}_2$  transformed transcripts per million. Boxes represent 25–75th percentile of expression and whiskers represent minimum and maximum data points. **C** Enriched pathways and DE genes in each pathway.

maintains the histomorphological features. RNA ISH was manually quantified globally and regionally (germinal center, mantle zone, and interfollicular zones). Some IL-6 expression was noted in the B cell rich mantle zones and germinal centers in all cases; however, it was significantly higher in interfollicular zones of MCD compared to UCD and reactive control lymph nodes (75% vs. 25% vs. 20%,  $p = 0.026$ ) (Fig. 4). Overall IL-6 expression was also higher in MCD as compared with UCD.

The presence of increased plasma cells in the interfollicular spaces of MCD lymph nodes suggested that they could be source of the elevated IL-6 expression. However, the histomorphological pattern of IL-6 RNA ISH was in scattered dispersed cells rather than clusters and sheets of plasma cells. In addition, dual RNAscope/IHC staining did not reveal significant co-expression of IL-6 and CD138 (Fig. 4A). The IL-6 expressing cells tracked along hypervascular areas in the interfollicular areas (Fig. 4B). IL-6 was overexpressed in

areas with CD31-positive endothelial or lymphatic structures. The findings suggest vasculature-associated cells, rather than plasma cells, as the major source of IL-6 in MCD.

**Increased VEGF expression by interfollicular histiocytes, follicular dendritic cells, and plasma cells in MCD**

Involvement of the VEGF pathway genes in MCD was noted by RNAseq analyses and prior studies.<sup>15,43</sup> Some VEGF expression in germinal centers and interfollicular areas was noted in both cases and controls. However, UCD and MCD showed increased expression compared to controls (Fig. 5). The proportion of strong expression, defined as 3+ or 4+ quantification, was strikingly increased in interfollicular areas and attenuated germinal centers of MCD compared to UCD or controls (75% vs. 29% vs. 0%;  $p = 0.014$ ) (Fig. 5B). Atretic follicles in CD are depleted of any lymphocytes and predominantly comprise follicular dendritic cells

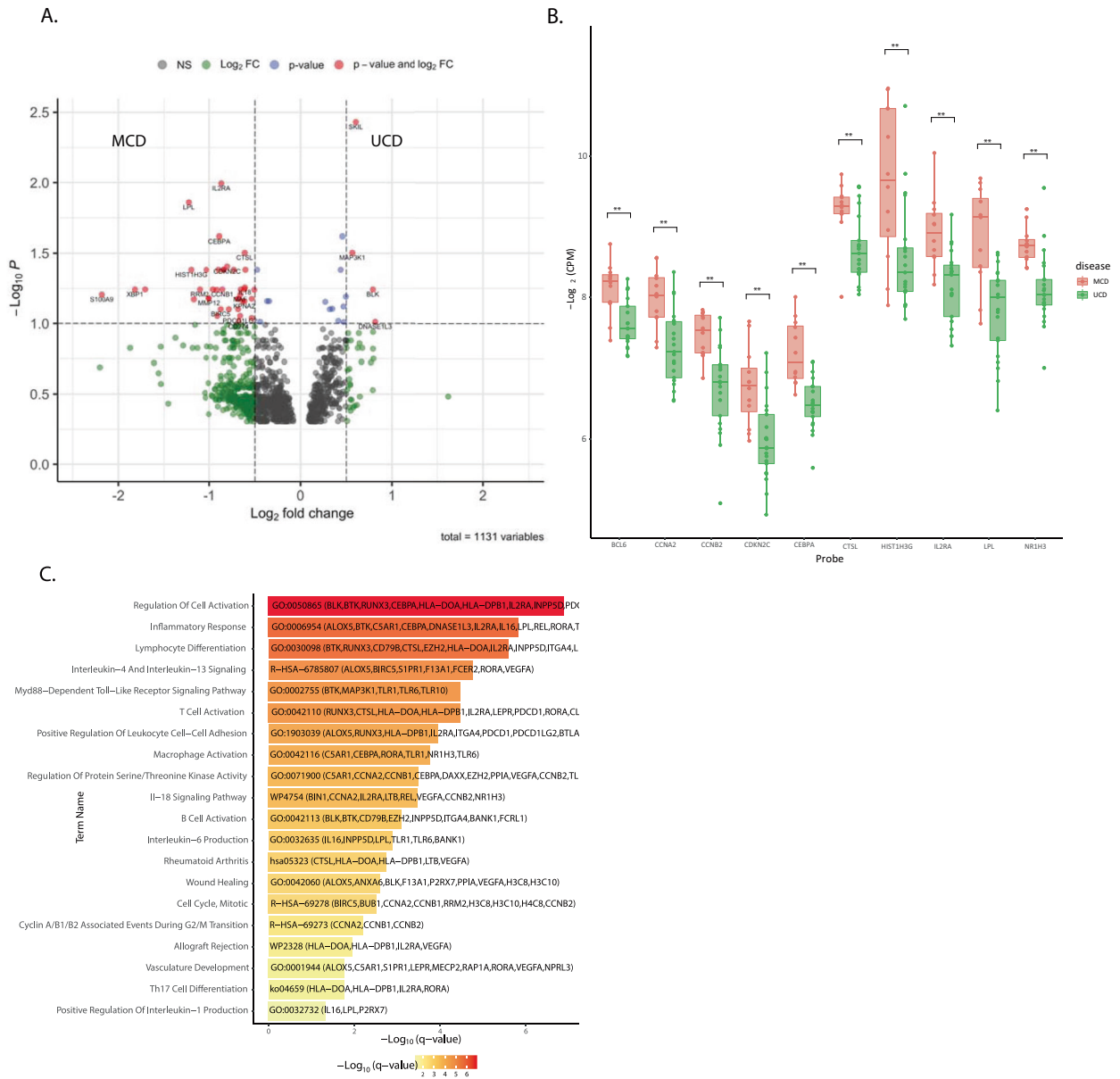


**Fig. 3 Unique genes and pathways of MCD compared to UCD. A** Volcano plot of significantly DE and upregulated genes. Genes in red represent those that satisfied log fold change > 0.5 and false discovery rate of 20%. **B** Box plots of top 10 DE genes upregulated in MCD versus UCD. Y axis represents log<sub>2</sub> transformed transcripts per million. Boxes represent 25–75th percentile of expression and whiskers represent minimum and maximum data points. **C** Enriched pathways and DE genes in each pathway.

(FDC). Dual RNAscope/IHC staining confirmed co-expression of VEGF and the FDC marker CD21 in attenuated germinal centers (Fig. 5A) that are devoid of other cell types. The predominant source of increased VEGF in the interfollicular zone was scattered macrophages with co-expression of M2 macrophage marker CD163 (Fig. 5B) and lacked co-expression with B cell marker CD20. Some cases showed VEGF expression in macrophages adjacent to blood vessels but not in endothelial cells. The findings implicate macrophage produced VEGF as potential contributors to the hypervascularity of CD. RNA ISH expression of IL-6R, IL-10, TNF $\alpha$ , IL-1 $\beta$ , IL-2, and IL-8 did not show significant differences between the various subtypes of CD.

**Immune repertoire of CD**

Given the reported activation of T cells in CD<sup>44</sup> and our findings of B cell activation in the RNAseq data, we analyzed the immune

repertoire of lymphocytes of eight UCD, eight MCD, and five control non-CD reactive lymph nodes by sequencing of TRB and IGH gene rearrangements (Fig. 6). Among TRB gene rearrangements, there was also a high degree of clonal diversity and minimal clonal expansion except for 2 MCD (cases 21 and 22) and 1 UCD (case 16) patients who exhibited clones that were at or above 3% of total copies and at least threefold higher than the next most frequent rearrangement (Fig. 6A). All samples exhibited a high degree of B cell diversity without significantly expanded (>2% of total sequence copies) clones except for MCD22 (Fig. 6B). To further evaluate immune repertoires for evidence of skewing or potential convergent selection in CD, we also analyzed the IGHV and TRBV gene usage. No significant VH gene skewing was observed in MCD or UCD compared to non-CD. We also analyzed somatic hypermutation frequencies in B cell sequencing data. UCD and MCD both showed less somatic hypermutation than non-CD

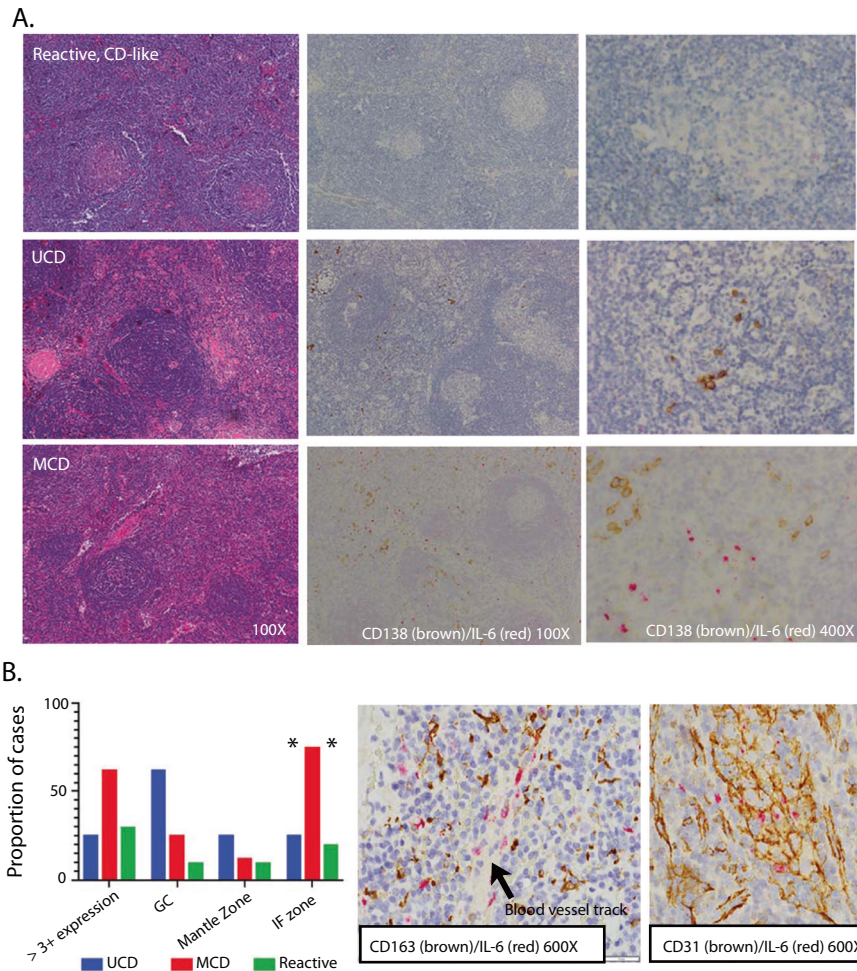


**Fig. 4** IL-6 expression by RNA ISH is elevated in MCD. **A** H&E and CD138(brown)/IL-6 (red) from a reactive Castleman-like lymph node case 27) (top panel), UCD case 9 (middle panel) and MCD case 25 (bottom panel). Increased IL-6 expression along interfollicular vascular structures and lack of co-expression with CD138 in MCD. IHC at 100 $\times$  and 400 $\times$  magnification are shown. **B** Spatial differences in IL-6 expression in CD and controls. Left: IL-6 expression was quantified within each lymph node region and compared across UCD, MCD, and reactive lymph nodes. IL-6 expression was significantly increased in the interfollicular space of MCD. Middle: IL-6 expression (red) in endothelial cells and lack of co-expression with histiocytic marker CD163 (MCD case 23) Right: IL-6 co expressed with endothelial marker CD31 (right, case 25) in the interfollicular hypervascular areas. IHC at 600 $\times$  magnification are shown. \* $P < 0.05$ .

reactive cases that may be consistent with B cell activation and germinal center depletion (Fig. 6C, D).

## DISCUSSION

In this study we characterized the transcriptome of UCD and MCD and determine the spatial localization of relevant cytokines. While prior sequencing studies investigated somatic mutations in DNA of patients with CD, we performed comparison of RNA expression patterns among groups of CD samples. This enabled identification of several unique genes and pathways involved in the pathogenesis of key histological features of UCD and MCD. A prominent histological feature of UCD that differentiates it from CD-like reactive nodes is hyalinization of the interfollicular space and vasculature. The presence of several extracellular matrix modifying genes among the top DE genes of UCD highlights the importance of remodeling processes. The most significant gene was SKIL which is a target of TGF $\beta$ . Upregulation of general inflammatory cytokines TGF $\beta$  and IL-1 $\beta$  could be linked to etiology of extracellular matrix remodeling in CD. Identification of FAS may be an indication of abnormalities of lymphocyte apoptosis in germinal centers. Interestingly, aberrancies of FAS and TGF $\beta$  were also reported in some cases of CD.<sup>21,45</sup> Another key morphological

feature of UCD is hypervascularity of the interfollicular space. Hence it is interesting that angiogenesis factors such as the notch ligand DLL4 and LPL were among the top DE genes. UCD shows depletion of germinal centers and thickened mantle zones that are suggestive of immune hyperactivation. The finding of B lymphocyte tyrosine kinase BLK and germinal center differentiation gene ZDHHC2 among the top DE genes highlight a potential role for B cell activation in pathogenesis. Shared germinal centers with FDC prominence is another key histologic feature of UCD. The presence of FDC markers and cytokines CXCL13 and clusterin among the top DE expressed genes suggest proliferation of FDC rather than relative prominence due to lymphodepletion. Pathway analysis also revealed a key C3-CXCL4-CXCL13-CXCL9-CXCL10 cytokine axis that may play an important role in the process. Since UCD group was predominantly composed of cases with hyaline vascular morphology, a histology based analysis showed similar results on our studies.

MCD shares some histological features with UCD. Hence, some genes and pathways such as FDC markers, angiogenesis and stromal remodeling factors were expected to be upregulated and DE in both. However, there were several pathways unique to MCD, particularly related to inflammation and immune activation. Prior studies show elevated serum levels of IL-6 in iMCD.<sup>46,47</sup> We show

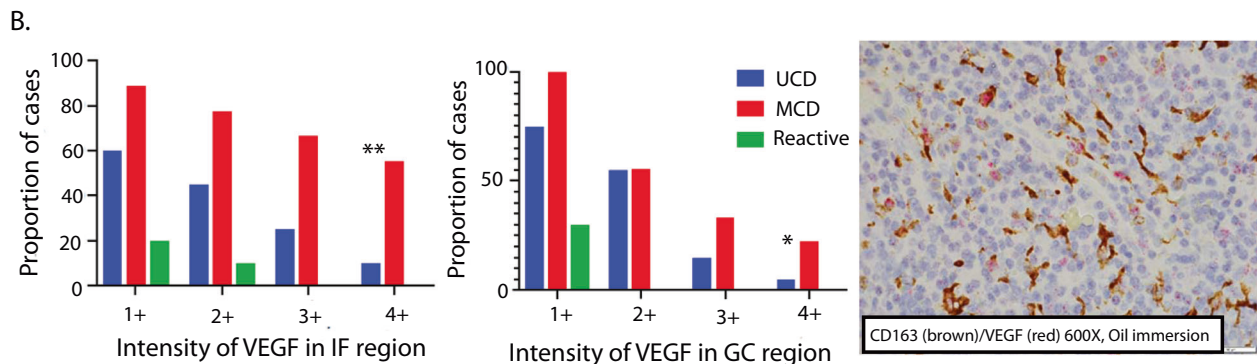
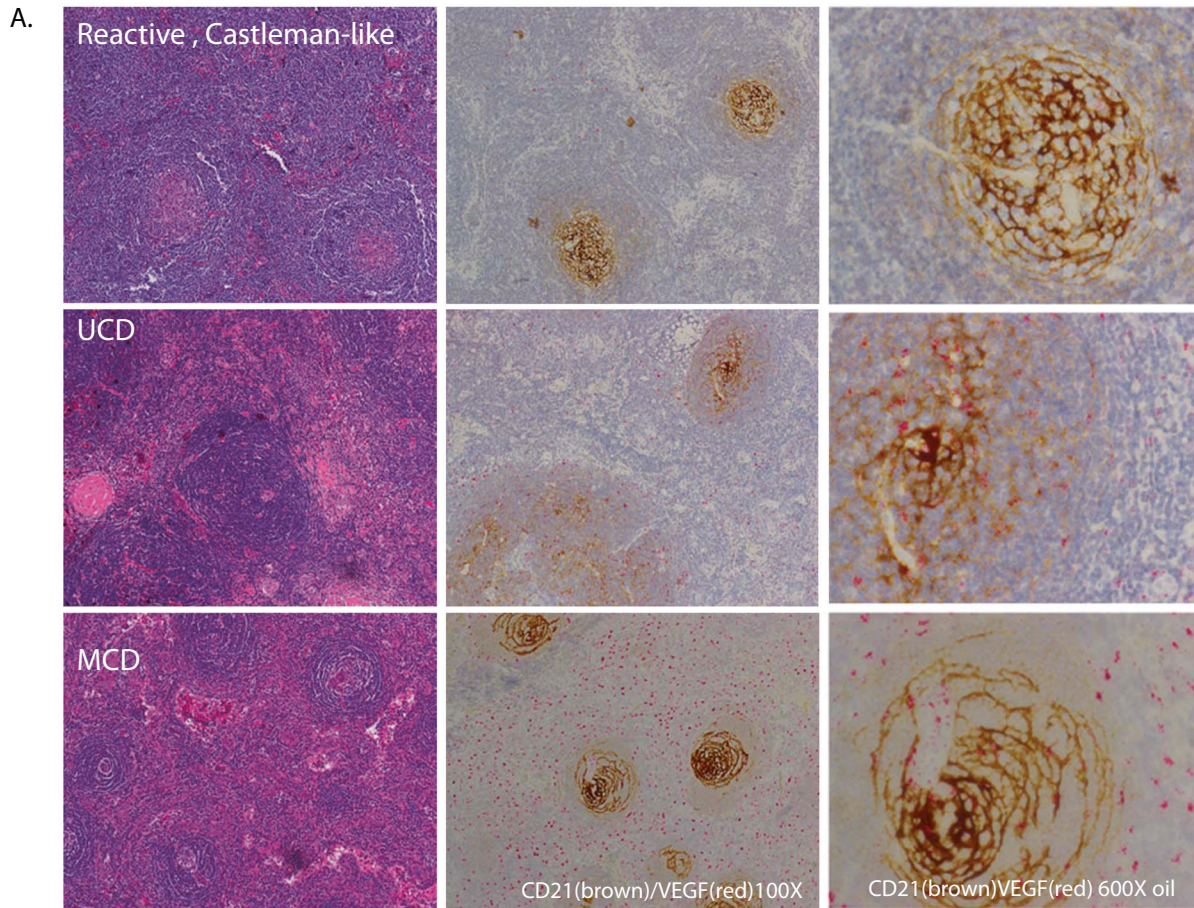


**Fig. 5 VEGF expression by RNA ISH is elevated in iMCD germinal centers and interfollicular areas.** **A** Top panel. H&E, and CD21(brown)/VEGF(red) from a reactive Castleman-like lymph node case 27 (upper panel), UCD case 9 (middle panel) and a MCD case 25 (bottom panel). IHC at 100x and 400x magnification are shown. Increased VEGF expression in the interfollicular areas and FDC-rich germinal centers of MCD. Scattered interfollicular expression in histiocytic cells with cytoplasmic projections. **B** VEGF expression by RNA ISH was elevated in iMCD germinal centers and interfollicular areas. Left and middle panels: VEGF expression by RNA ISH was significantly stronger in MCD in cells within the interfollicular space and germinal center. Right panel: Co-expression of histiocyte specific marker CD163 (brown IHC) with VEGF (red, RNA ISH) in MCD case 23. IHC at 600x magnification are shown.

for the first time that multiple IL-6 associated genes and pathways were uniquely upregulated in lymph nodes from patients with MCD. B cells and plasma cells were initially thought to be the source of IL-6 expression within the germinal center.<sup>47</sup> However, subsequent studies implicated monocytes, follicular dendritic cells, and endothelial cells as well.<sup>46,48,49</sup> Prior studies utilized IHC to identify IL-6 expression in plasma cells and vascular endothelial cells in cases of “plasma cell CD”.<sup>50</sup> IL-6 causes downstream effects by activation, differentiation and proliferation of macrophages, lymphocytes and platelets respectively. IL-6 is also a growth factor for plasma cells and is required for generation

of long-lived plasma cells.<sup>51</sup> In this context, it is interesting that plasma cell differentiation molecule XBP1 was one of the top overexpressed genes in MCD. Plasma cell differentiation pathways were also identified by gene set enrichment analysis. In order to clarify the source of IL-6, VEGF and other cytokines, we utilized RNA ISH to assess the histomorphological pattern of cytokine expression in CD lymph nodes and controls. We found that IL-6 was increased in the interfollicular areas of MCD cases compared to UCD, a finding that was previously seen by immunohistochemistry as well.<sup>50</sup> We extended those observations and showed that IL-6 was not co-expressed with plasma cells but tracked along

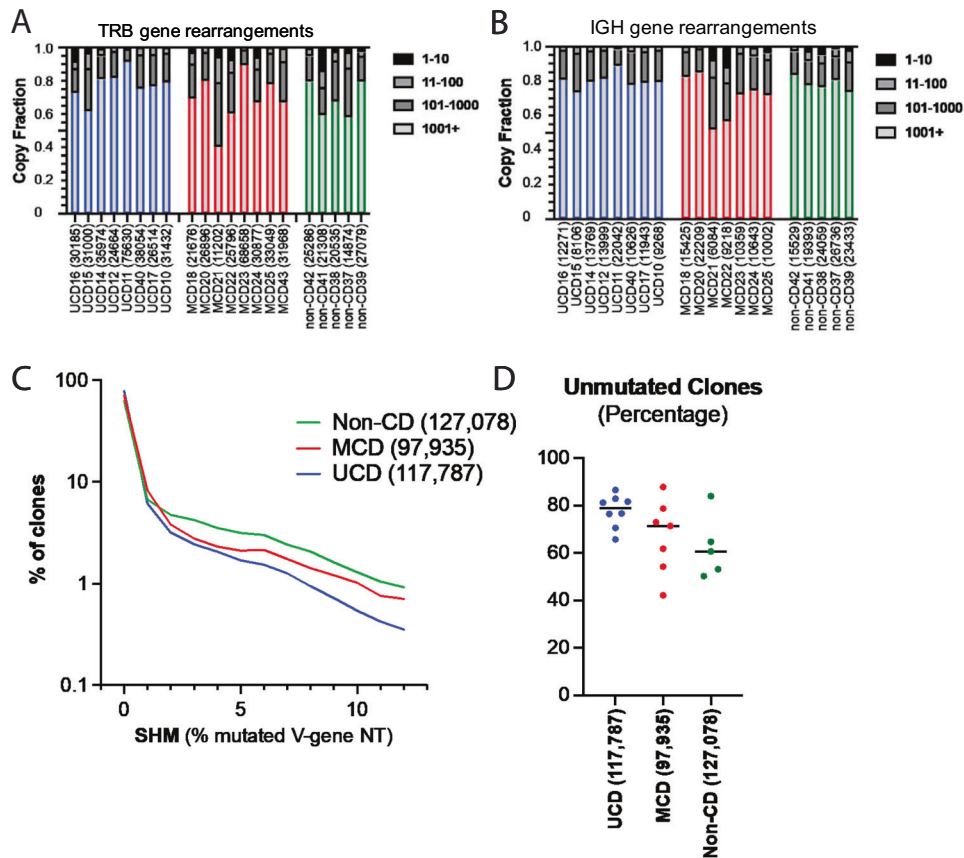


**Fig. 6 IGH and TRB gene rearrangement analysis.** **A** Clone size rank plots of TRB gene rearrangement. TRB gene rearrangements were grouped into clonotypes (see methods) and ranked by copy number into bins corresponding to the top 10 ranked clones, 11–100, 101–1000 and >1000. The copy number fractions of clones falling into the binned size ranges are shown for each individual. Total clone counts for each individual are given in parenthesis. **B** Clone size rank plots of IGH gene rearrangement. Expanded clones are shaded in solid black. **C** Distribution of somatic hypermutation (SHM) levels (percentage of mutated nucleotides, NT, away from the nearest germline IGHV gene). Data are visualized on a log<sub>10</sub> scale to reveal the different levels of SHM between the populations. Clone counts, summed for all of the individuals in each diagnostic category, are given in parentheses. Median SHM levels are statistically significant between each population ( $p < 0.0001$ , Mann Whitney two-sided test). **D** Fraction of clones without SHM (< 0.5% mutation in the IGHV gene compared to the nearest germline gene).

CD31 expressing vascular structures that could be of endothelial or lymphatic origin. The findings suggest vasculature-associated cells may be a significant source of IL-6 in CD with the caveat that Angiomyoid stromal cell populations are hypothesized to be involved in the pathogenesis of CD.<sup>16,52</sup> The identification of the fibroblastic reticulum cell marker and cytokine CCL21 as one the top DE genes identifies it as another stromal cell of interest in CD.

IL-6 can also induce VEGF secretion. VEGF is upregulated in iMCD.<sup>43</sup> Lymph node vascularity and eruptive cherry hemangiomas are attributed to VEGF.<sup>8,53</sup> Similar to IL-6, VEGF is produced by many cell types including macrophages, platelets, and plasma cells. We showed for the first time the upregulation of VEGF and angiogenesis pathways in lymph nodes involved by MCD. We identified increased VEGF by RNA ISH in the interfollicular areas and attenuated germinal centers. FDCs were the source of increased VEGF within the attenuated germinal centers while interfollicular source of VEGF appear to be mainly CD163-positive M2-like macrophages, and plasma cells by immunohistochemistry and morphology. Increased expression of VEGF was noted in UCD as well but was highest in MCD. The identification of FDCs as a major source of VEGF is interesting given that dysplastic FDCs with cytogenetic abnormalities have been noted in CD.<sup>16,52</sup> PDGFRB mutations have also been noted in CD45-negative stromal compartment of UCD.<sup>24</sup> CXCL13 and clusterin overexpression in both UCD and MCD further suggest the importance of FDCs. Our findings supports the hypothesis that CD may be driven by a

neoplastic cell. However, we cannot completely rule out an autoimmune etiology. Single cell sequencing techniques and multiplex imaging techniques are necessary to confirm the identity and genetics of IL-6 and VEGF-expressing cell populations.

IL-6 pathway inhibitors are already used to treat MCD.<sup>54</sup> VEGF- or TGF $\beta$ -inhibitors that were developed for oncologic indications may be investigated for use in CD. While immune response and lymphocyte activation pathways were enriched in both UCD and MCD, MTORC1 and allograft response pathways were unique to MCD. MTOR inhibitors such sirolimus and tacrolimus are commonly used for immunosuppression after solid organ transplant to block T cell activation. Populations of activated CD8<sup>+</sup> T cells have been identified in iMCD disease flares.<sup>55</sup> Increased mTOR activation has been noted in iMCD<sup>44,55</sup> and forms the basis of a trial investigating sirolimus in MCD (NCT03933904). Immunoglobulin light and heavy chain restriction and clonal immunoglobulin gene rearrangements have been noted occasionally in plasma cell predominant and multicentric variants of CD.<sup>17,56</sup> To our knowledge, this is the first study to utilize deep sequencing to analyze lymphocyte populations within lymph nodes of CD patients. Some cases of CD demonstrated minor expansions of T cell clones that are consistent with T-cell activation seen in transcriptome analysis. However, in a lymph node sample, sometimes clones of this size can be encountered in healthy individuals as well.<sup>57</sup> Higher frequencies of unmutated clones in UCD and MCD are likely due to depletion of normal

germinal center B cells and expansion of mantle zones. The IGH and TRB findings further support the morphological and transcriptome findings of immune hyperactivation in CD lymph nodes.

In conclusion, we have identified the genes, pathways and cell types that may be important to the pathogenesis of UCD and MCD. The findings provide mechanistic insights and suggest novel diagnostic modalities and therapeutic options to target these genes and pathways.

## DATA AVAILABILITY

Data generated or analyzed during this study are included in this published article (and its supplementary information files). Raw TRB and IGH gene rearrangement data are available on SRA under project number PRJNA750097. Any other data will be provided on reasonable request to corresponding author.

## REFERENCES

- Sopfe, J. et al. Castleman disease in pediatrics: Insights on presentation, treatment, and outcomes from a two-site retrospective cohort study. *Pediatr. Blood Cancer* **66**, e27613 (2019).
- Talat, N., Belgaumkar, A. P. & Schulte, K. M. Surgery in Castleman's disease: a systematic review of 404 published cases. *Ann. Surg.* **255**, 677–684 (2012).
- Zhang, M. Y. et al. UCD with MCD-like inflammatory state: surgical excision is highly effective. *Blood Adv.* **5**, 122–128 (2021).
- van Rhee, F. et al. International evidence-based consensus diagnostic and treatment guidelines for unicentric Castleman disease. *Blood Adv.* **4**, 6039–6050 (2020).
- Dispenzieri, A. et al. The clinical spectrum of Castleman's disease. *Am. J. Hematol.* **87**, 997–1002 (2012).
- Dispenzieri, A. & Fajgenbaum, D. C. Overview of Castleman disease. *Blood* **135**, 1353–1364 (2020).
- Fajgenbaum, D. C. et al. Insufficient evidence exists to use histopathologic subtype to guide treatment of idiopathic multicentric Castleman disease. *Am. J. Hematol.* **95**, 1553–1561 (2020).
- Fajgenbaum, D. C. et al. International, evidence-based consensus diagnostic criteria for HHV-8-negative/idiopathic multicentric Castleman disease. *Blood* **129**, 1646–1657 (2017).
- Fajgenbaum, D. C., Van Rhee, F. & Nabel, C. S. HHV-8-negative, idiopathic multicentric Castleman disease: Novel insights into biology, pathogenesis, and therapy. *Blood* **123**, 2924–2933 (2014).
- Pierson, S. K. et al. Plasma proteomics identifies a 'chemokine storm' in idiopathic multicentric Castleman disease. *Am. J. Hematol.* **93**, 902–912 (2018).
- Aoki, Y. et al. Angiogenesis and hematopoiesis induced by Kaposi's sarcoma-associated herpesvirus-encoded interleukin-6. *Blood* **93**, 4034–4043 (1999).
- Suda, T. et al. HHV-8 infection status of AIDS-unrelated and AIDS-associated multicentric castleman's disease. *Pathol. Int.* **51**, 671–679 (2001).
- Nishimoto, N. et al. Humanized anti-interleukin-6 receptor antibody treatment of multicentric Castleman disease. *Blood* **106**, 2627–2632 (2005).
- van Rhee, F. et al. Siltuximab for multicentric Castleman's disease: a randomised, double-blind, placebo-controlled trial. *Lancet Oncol.* **15**, 966–974, [https://doi.org/10.1016/S1470-2045\(14\)70319-5](https://doi.org/10.1016/S1470-2045(14)70319-5) (2014).
- Nishi, J. et al. Expression of vascular endothelial growth factor in sera and lymph nodes of the plasma cell type of Castleman's disease. *Br. J. Haematol.* **104**, 482–485 (1999).
- Chen, W. C. et al. Cytogenetic anomalies in hyaline vascular Castleman disease: Report of two cases with reappraisal of histogenesis. *Cancer Genet. Cytogenet.* **164**, 110–117 (2006).
- Radaszkiewicz, T., Lennert, K. & Hansmann, M.-L. Monoclonality and polyclonality of plasma cells in Castleman's disease of the plasma cell variant. *Histopathology* **14**, 11–24, <https://doi.org/10.1111/j.1365-2559.1989.tb02110.x> (1989).
- Wang, H. W., Pittaluga, S. & Jaffe, E. S. Multicentric Castleman disease: Where are we now? *Semin. Diagnostic Pathol.* **33**, 294–306 (2016).
- Chang, K. C. et al. Monoclonality and cytogenetic abnormalities in hyaline vascular Castleman disease. *Mod. Pathol.* **27**, 823–831 (2014).
- Baker, T. S. et al. A novel FAS mutation with variable expressivity in a family with unicentric and idiopathic multicentric Castleman disease. *Blood Adv.* **2**, 2959–2963 (2018).
- Nagy, A. et al. Next-generation sequencing of idiopathic multicentric and unicentric Castleman disease and follicular dendritic cell sarcomas. *Blood Adv.* **2**, 481–491 (2018).
- Endo, Y. et al. Mediterranean fever gene variants modify clinical phenotypes of idiopathic multi-centric Castleman disease. *Clin. Exp. Immunol.* **206**, 91–98, <https://doi.org/10.1111/cei.13632> (2021).
- You, L. et al. Whole-exome sequencing identifies novel somatic alterations associated with outcomes in idiopathic multicentric Castleman disease. *Br. J. Haematol.* **188**, e64–e67 (2020).
- Li, Z. et al. Recurrent PDGFRB mutations in unicentric Castleman disease. *Leukemia* **33**, 1035–1038 (2019).
- Qi, Z. et al. Reliable gene expression profiling from small and hematoxylin and eosin-stained clinical formalin-fixed, paraffin-embedded specimens using the HTG EdgeSeq platform. *J. Mol. Diagn.* **21**, 796–807 (2019).
- Godoy, P. M. et al. Comparison of reproducibility, accuracy, sensitivity, and specificity of miRNA quantification platforms. *Cell Rep.* **29**, 4212–4222.e4215 (2019).
- Zhang, L. et al. Cross-platform comparison of immune-related gene expression to assess intratumor immune responses following cancer immunotherapy. *J. Immunol. Methods* **494**, 113041 (2021).
- Wang, L. et al. EMT- and stroma-related gene expression and resistance to PD-1 blockade in urothelial cancer. *Nat. Commun.* **9**, 3503 (2018).
- Ritchie, M. E. et al. limma powers differential expression analyses for RNA-sequencing and microarray studies. *Nucleic Acids Res.* **43**, e47 (2015).
- Zhou, Y. et al. Metascape provides a biologist-oriented resource for the analysis of systems-level datasets. *Nat. Commun.* **10**, 1523 (2019).
- Subramanian, A. et al. Gene set enrichment analysis: a knowledge-based approach for interpreting genome-wide expression profiles. *Proc. Natl Acad. Sci. USA* **102**, 15545–15550 (2005).
- Szklarczyk, D. et al. STRING v10: protein-protein interaction networks, integrated over the tree of life. *Nucleic Acids Res.* **43**, D447–D452 (2015).
- Bader, G. D. & Hogue, C. W. An automated method for finding molecular complexes in large protein interaction networks. *BMC Bioinform.* **4**, 2 (2003).
- Leick, M. et al. T cell clonal dynamics determined by high-resolution tcr-Beta sequencing in recipients after allogeneic hematopoietic cell transplantation. *Biol. Blood Marrow Transpl.* **26**, 1567–1574 (2020).
- Meng, W. et al. An atlas of B-cell clonal distribution in the human body. *Nat. Biotechnol.* **35**, 879–884 (2017).
- Miron, M., et al. Human lymph nodes maintain quiescent memory T cells with high functional potential and clonal diversity throughout life. *J. Immunol.* **201**, 2132–2140 (2021).
- Rosenfeld, A. M., Meng, W., Luning Prak, E. T. & Hershberg, U. ImmuneDB, a novel tool for the analysis, storage, and dissemination of immune repertoire sequencing data. *Front. Immunol.* **9**, 2107 (2018).
- Miron, M. et al. Maintenance of the human memory T cell repertoire by subset and tissue site. *Genome Med.* **13**, 100 (2021).
- Ye, J., Ma, N., Madden, T. L. & Ostell, J. M. IgBLAST: an immunoglobulin variable domain sequence analysis tool. *Nucleic Acids Res.* **41**, W34–W40 (2013).
- Kuri-Cervantes, L. et al. Comprehensive mapping of immune perturbations associated with severe COVID-19. *Sci. Immunol.* **5**, (49) (2020).
- Oksenhendler, E. et al. The full spectrum of Castleman disease: 273 patients studied over 20 years. *Br. J. Haematol.* **180**, 206–216 (2018).
- Chisholm, K. M. & Fleming, M. D. Histologic and laboratory characteristics of symptomatic and asymptomatic Castleman disease in the pediatric population. *Am. J. Clin. Pathol.* **153**, 821–832 (2020).
- Nishi, J. I. & Maruyama, I. Increased expression of vascular endothelial growth factor (VEGF) in Castleman's disease: proposed pathomechanism of vascular proliferation in the affected lymph node. *Leuk. Lymphoma* **38**, 387–394 (2000).
- Arenas, D. J. et al. Increased mTOR activation in idiopathic multicentric Castleman disease. *Blood* **135**, 1673–1684 (2020). May 7(2020-1684).
- Baker, T. S. et al. A novel. *Blood Adv.* **2**, 2959–2963 (2018).
- Leger-Ravet, M. B. et al. Interleukin-6 gene expression in Castleman's disease. *Blood* **78**, 2923–2930 (1991).
- Yoshizaki, K. et al. Pathogenic Significance of Interleukin-6 (IL-6/BSF-2) in Castleman's Disease. *Blood* **74**, 1360–1367 (1989).
- Ishiyama, T. et al. Immunodeficiency and IL-6 production by peripheral blood monocytes in multicentric Castleman's disease. *Br. J. Haematol.* **86**, 483–489 (1994).
- Lai, Y.-m et al. Expression of interleukin-6 and its clinicopathological significance in Castleman's disease. *Chin. J. Hematol.* **34**, 404–408 (2013).
- Post, G. R. et al. Diagnostic utility of interleukin-6 expression by immunohistochemistry in differentiating castleman disease subtypes and reactive lymphadenopathies. *Ann. Clin. Lab. Sci.* **46**, 474–479 (2016).
- Jourdan, M. et al. IL-6 supports the generation of human long-lived plasma cells in combination with either APRIL or stromal cell-soluble factors. *Leukemia* **28**, 1647–1656 (2014).
- Lin, O. & Frizzera, G. Angiomyoid and follicular dendritic cell proliferative lesions in Castleman's disease of hyaline-vascular type: a study of 10 cases. *Am. J. Surg.*

- Pathol.* **21**, 1295–1306, <https://doi.org/10.1097/0000478-199711000-00004> (1997).
53. Fajgenbaum, D., Rosenbach, M., Van Rhee, F., Nasir, A. & Reutter, J. Eruptive cherry hemangiomas associated with multicentric Castleman disease: a case report and diagnostic clue. *JAMA Dermatol.* **149**, 204–208 (2013).
  54. van Rhee, F. et al. International, evidence-based consensus treatment guidelines for idiopathic multicentric Castleman disease. *Blood* **132**, 2115–2124 (2018).
  55. Pai, R. L., et al. Type I IFN response associated with mTOR activation in the TAFRO subtype of idiopathic multicentric Castleman disease. *JCI Insight* **5**, May 7;5: e135031 (2020).
  56. Ohyashiki, J. H. et al. Molecular genetic, cytogenetic, and immunophenotypic analyses in Castleman's disease of the plasma cell type. *Am. J. Clin. Pathol.* **101**, 290–295, <https://doi.org/10.1093/ajcp/101.3.290> (1994).
  57. Kussick, S. J., Kalnoski, M., Brazier, R. M. & Wood, B. L. Prominent clonal B-cell populations identified by flow cytometry in histologically reactive lymphoid proliferations. *Am. J. Clin. Pathol.* **121**, 464–472 (2004).

## ACKNOWLEDGEMENTS

We would like to thank Dan Martinez, the CHOP pathology core and the Human Immunology Core laboratories for technical support. We would like to thank Ms. Rachel Olson and Mr. Brian Lockhart for administrative support.

## AUTHOR CONTRIBUTIONS

V.P. performed study concept and design; A.W., D.F., M.S.L., E.L.P., D.T.T., D.C.F. and V.P. performed writing, review and revision of the paper; A.W., J.X., W.M., A.M.M.,

E.Y.L., K.T., D.T.T., D.C.F., and V.P. provided acquisition, analysis and interpretation of data, and statistical analysis; G.W., M.P., D.F., A.B., D.T.T., M.S.L. and D.C.F. provided material support. All authors read and approved the final paper.

## FUNDING

V.P. received research funding from the Castleman Disease Collaborative Network. V.P. is the recipient of an autoimmune research grant from HTG Molecular Diagnostics, Inc. E.L.P., W.M., and A.M.R. are funded by NIH P30-CA016520.

## COMPETING INTERESTS

The authors do not have a conflict of interest.

## ADDITIONAL INFORMATION

**Supplementary information** The online version contains supplementary material available at <https://doi.org/10.1038/s41379-021-00950-3>.

**Correspondence** and requests for materials should be addressed to Vinodh Pillai.

**Reprints and permission information** is available at <http://www.nature.com/reprints>

**Publisher's note** Springer Nature remains neutral with regard to jurisdictional claims in published maps and institutional affiliations.